Origin and stability of the dipolar response in a family of tetragonal tungsten bronze relaxors

Andrei Rotaru,[1] Donna C. Arnold,[1] Aziz Daoud-Aladine,[2] and Finlay D. Morrison[1,*]

[1]*EaStCHEM School of Chemistry, University of St. Andrews, North Haugh, St. Andrews, Fife KY16 9ST, United Kingdom*

[2]*ISIS Facility, Rutherford Appleton Laboratory, Chilton, Didcot OX11 0QX, United Kingdom*

(Received 23 December 2010; revised manuscript received 25 March 2011; published 31 May 2011)

A new family of relaxor dielectrics with the tetragonal tungsten bronze structure (nominal composition $Ba_6M^{3+}Nb_9O_{30}$, M^{3+} = Ga, Sc, or In) were studied using dielectric spectroscopy to probe the dynamic dipole response and correlate this with the crystal structure as determined from powder neutron diffraction. Independent analyses of real and imaginary parts of the complex dielectric function were used to determine characteristic temperature parameters, T_{VF} and T_{UDR}, respectively. In each composition both these temperatures correlated with the temperature of maximum crystallographic strain, $T_{c/a}$, determined from diffraction data. The overall behavior is consistent with dipole freezing and the data indicate that the dipole stability increases with increasing M^{3+} cation size as a result of increased tetragonality of the unit cell. Crystallographic data suggests that these materials are uniaxial relaxors with the dipole moment predominantly restricted to the $B1$ cation site in the structure. Possible origins of the relaxor behavior are discussed.

DOI: 10.1103/PhysRevB.83.184302 PACS number(s): 77.22.Gm, 77.80.Jk, 61.05.fg

I. INTRODUCTION

In recent years there has been a resurgence in research dedicated to the discovery of novel ferroelectric materials primarily due to the combination of the requirement of Pb-free alternatives to $PbZr_xTi_{1-x}O_3$ (PZT) (Ref. 1) and the recent renaissance in multiferroics.[2] To date, much of the search for new materials has largely centered on perovskite (ABO_3) -based materials such as $K_{1-x}Na_xNbO_3$ (as a Pb-free piezoelectric)[3] and $BiFeO_3$ (the most well-known room-temperature multiferroic)[4] due to both their compositional flexibility and also our level of understanding of mechanisms to tune properties in this structure type; simple arguments based on steric considerations (tolerance factor), cation and charge ordering, and octahedral tilting are all tools to be exploited in the quest for new perovskite ferroelectric and multiferroic materials. More recently, an emerging class of materials, tetragonal tungsten bronzes (TTB), has begun to garner renewed interest in the research community. These materials are known to exhibit diverse properties as a result of compositional flexibility, however, while ferroelectric TTBs [including $Ba_2NaNb_5O_{15}$ (Refs. 5–7) and $(Ba,Sr)Nb_2O_6$ (Refs. 8–10)] were widely studied in the 1960s and 1970s, our understanding of the manipulation of this structure type is still poor compared to perovskites.

The TTB structure, $A1_2A2_4C_4B1_2B2_8O_{30}$, is closely related to the perovskite structure, however, the presence of crystallographically nonequivalent A and B sites and an extra C site provide extra degrees of freedom for manipulation of the structure offering huge compositional flexibility.[11] The TTB structure consists of a network of corner-sharing BO_6 octahedra (Fig. 1, inset), which form perovskite ($A1$) and pentagonal ($A2$) channels which can be occupied by alkali, alkaline earth, and rare-earth cations. Smaller triangular (C) channels are also formed and while in many TTBs these sites are vacant, they can be filled (or partially filled) by small low-charged cations such as Li^+ (e.g., $K_6Li_4Nb_{10}O_{30}$).[12]

Much of the focus on recent TTB materials has been directed at $Ba_6Ti_2Nb_8O_{30}$ (Ref. 13) and its doped analogs as a result of both Ti^{4+} and Nb^{5+} being considered to be ferroelectrically active ions and the high Curie temperatures, T_C, (~500 K) observed in these materials. Isovalent replacement of the Ba^{2+} cation with either Sr^{2+} and/or Ca^{2+} has been shown to result in changes in symmetry and thus shift the value of T_C.[14] Neurgaonkar *et al.* reported that $Sr_6Ti_2Nb_8O_{30}$ was orthorhombic in structure in comparison with $Ba_6Ti_2Nb_8O_{30}$, which is tetragonal[14] with a minimum in T_C observed at ca. 70 mol % Sr substitution which they associated with a morphotropic phase boundary between the Ba-rich tetragonal phases and orthorhombic Sr-rich compositions. Furthermore, they demonstrated that the addition of Ca^{2+} stabilized the orthorhombic distortion. The effects of incorporation of larger valence cations such as Bi^{3+} and RE^{3+} [RE = La, Pr, Nd, Sm, Eu, Gd, or Dy (where RE stands for rare earth)] onto the A site, through cooperative doping with Ti^{4+} on the B site, has also been reported.[15–18] It has been shown that while incorporation of La^{3+} or Bi^{3+} into the structure results in relaxor-type ferroelectric character, incorporation of the smaller rare earths results in classic ferroelectric behavior.[15,16] More recently it has been suggested that the ferroelectric behavior in these materials is dominated by the A-site cations and in particular, by the ionic radius difference between the ions on the $A1$ and $A2$ sites.[19]

The incorporation of nonferroelectrically active species, such as Fe^{3+}, Ni^{2+}, and Mg^{2+}, into the TTB framework has also been reported.[20–23] For rare-earth-substituted $Ba_6FeNb_9O_{30}$ studies have shown the size of the RE ion to have a large influence on the observed properties.[24,25] However, in contrast, little work has been undertaken in understanding the effects of B-site doping on the observed ferroelectric and dielectric properties. Replacement of Ti^{4+} in ferroelectric $Ba_6Ti_2Nb_8O_{30}$ TTBs with Sn^{4+}, Zr^{4+}, or Hf^{4+} has demonstrated that T_C decreases with increasing cell volume (M^{4+} ionic radius).[13,14] In contrast, we recently showed that increasing the ionic radii of M^{3+} ions in $Ba_6M^{3+}Nb_9O_{30}$ TTBs (M = Ga^{3+}, Fe^{3+}, Sc^{3+}, In^{3+} or Y^{3+}) results in an increase in the polar stability.[26] These observations can more readily be described by tetragonality (c/a) such that irrespective of the valence of the metal ion in the TTB the transition temperature increases with increasing tetragonality (strain).[26] These

observations marked steps towards quantitatively correlating the compositional-structure-property relations in TTBs so that a "global" understanding of these materials similar to those in perovskites can be utilized in the design of new materials. This is an important step if novel materials of this structure type are to be fully exploited for future applications.

In this paper we report full structural and dielectric characterization of $Ba_6M^{3+}Nb_9O_{30}$ (M^{3+} = Ga, Sc, or In) TTB materials. All materials exhibit dielectric permittivity and loss curves typical of relaxor behavior. Characteristic temperature parameters for each sample were extracted from both dielectric and crystallographic data as a function of temperature: Vogel-Fulcher fitting of the maximum in dielectric constant to determine the Vogel-Fulcher temperature, T_{VF}; T_{UDR} corresponding to absolute flattening of the dielectric loss peak in the frequency domain; and $T_{c/a}$ corresponding to the maximum crystallographic tetragonal strain. These temperatures coincided for each composition investigated and furthermore increased with increasing strain induced by an increase in the M^{3+} cation size. These observations are consistent with slowing of dipoles on cooling and eventual "locking" of the *B*-cation displacements along the *c* axis, i.e. dipole freezing.

II. EXPERIMENTAL

Samples with the composition $Ba_6M^{3+}Nb_9O_{30}$ (where M^{3+} = Ga, Sc, or In) were prepared as described previously.[26] Briefly, stoichiometric ratios of $BaCO_3$, Nb_2O_5, Ga_2O_3, In_2O_3 (all Aldrich, 99+%), and Sc_2O_3 (Stanford Materials Corporation, 99.999%) were ball milled and subjected to the following heating regime: 4 h at 1000 °C, 10 h at 1250 °C followed by ball milling, and 6 h at 1350 °C (1300 °C for $Ba_6GaNb_9O_{30}$). Phase formation was confirmed by powder x-ray diffraction collected over a range of 20 to 60 in transmission mode using a STOE diffractometer with Cu $K\alpha_1$ radiation (40 kV and 30 mA, λ = 1.5405 Å). Powder neutron diffraction measurements were conducted on the high-resolution powder diffractometer (HRPD) at ISIS. Data were collected at temperatures between 10 and 450 K using a closed cycle refrigerator (CCR) with the materials loaded into aluminum cells fitted with vanadium windows. Pellets were prepared for electrical characterization at 1350 °C (1300 °C for $Ba_6GaNb_9O_{30}$) and all exhibited >90% theoretical density. Pt electrodes were applied using Pt paste (Gwent Electronic Materials Ltd.) and cured at 900 °C for approximately 20 min. Dielectric measurements were made using an Agilent 4294A impedance analyzer over a frequency range of ca. 100 Hz–5 MHz and a temperature range of approximately 50–340 K with cooling/heating rates of 2 K min^{-1} and applied ac excitation of 500 mV.

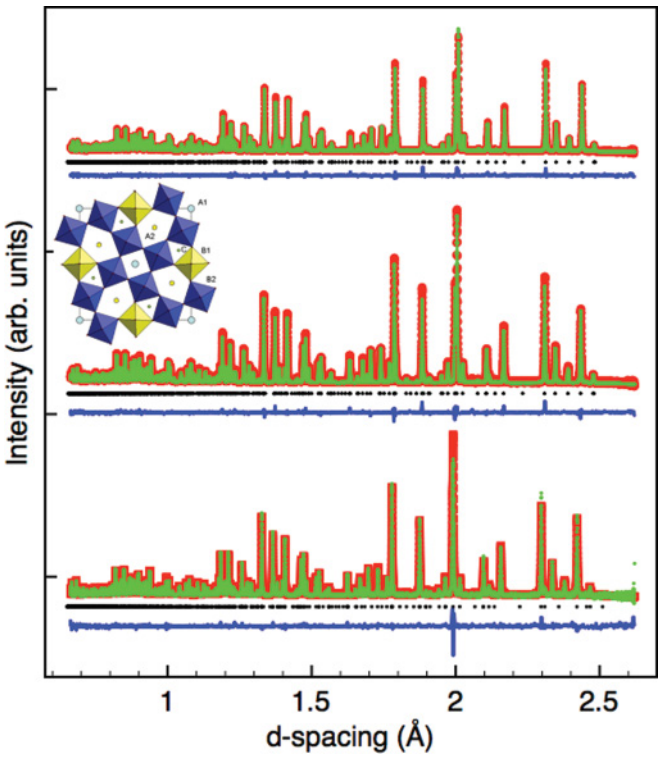

FIG. 1. (Color online) Rietveld refinements in centrosymmetric tetragonal space group $P4/mbm$ of room-temperature powder neutron data for $Ba_6GaNb_9O_{30}$ (bottom), $Ba_6ScNb_9O_{30}$ (middle), and $Ba_6InNb_9O_{30}$ (top). (Inset: TTB structure with *B*1 and *B*2 octahedra shown in yellow and blue, respectively.)

III. RESULTS

A. General observations

Room-temperature powder neutron diffraction (PND) indicated that all three compounds form the TTB phase with a small amount of minor perovskite-related phase, $Ba_5Nb_4O_{15}$. All three were refined in the space group $P4/mbm$ (No. 127) using the Rietveld method, Fig. 1, and Table I (see supplemental material[57]). A systematic increase in lattice parameters and unit-cell volume was observed with increasing ionic radius of the M^{3+} *B*-site cation ($r_{Ga^{3+}} = 0.62 < r_{Sc^{3+}} = 0.745 < r_{In^{3+}} = 0.80$ Å for sixfold coordination[27]), in good agreement with our previous x-ray diffraction study.[26] The amount of second phase was determined from dual phase refinements and was found to be approximately 10% in $Ba_6GaNb_9O_{30}$ and 6% in $Ba_6ScNb_9O_{30}$. No secondary phases were observed

TABLE I. Unit-cell dimensions and goodness-of-fit parameters for $Ba_6M^{3+}Nb_9O_{30}$ ($M^{3+} = Ga^{3+}$, Sc^{3+}, In^{3+}) refined from PND data at 300 K in space group $P4/mbm$.

	a (Å)	c (Å)	V (Å^3)	R_p (%)	wR_p (%)	χ^2
$Ba_6GaNb_9O_{30}$	12.5723(3)	3.98181(2)	629.384(4)	6.04	6.19	13.46
$Ba_6ScNb_9O_{30}$	12.63011(2)	4.00746(1)	639.268(3)	4.35	4.77	8.542
$Ba_6InNb_9O_{30}$	12.64713(2)	4.01688(1)	642.500(3)	4.31	4.81	7.248

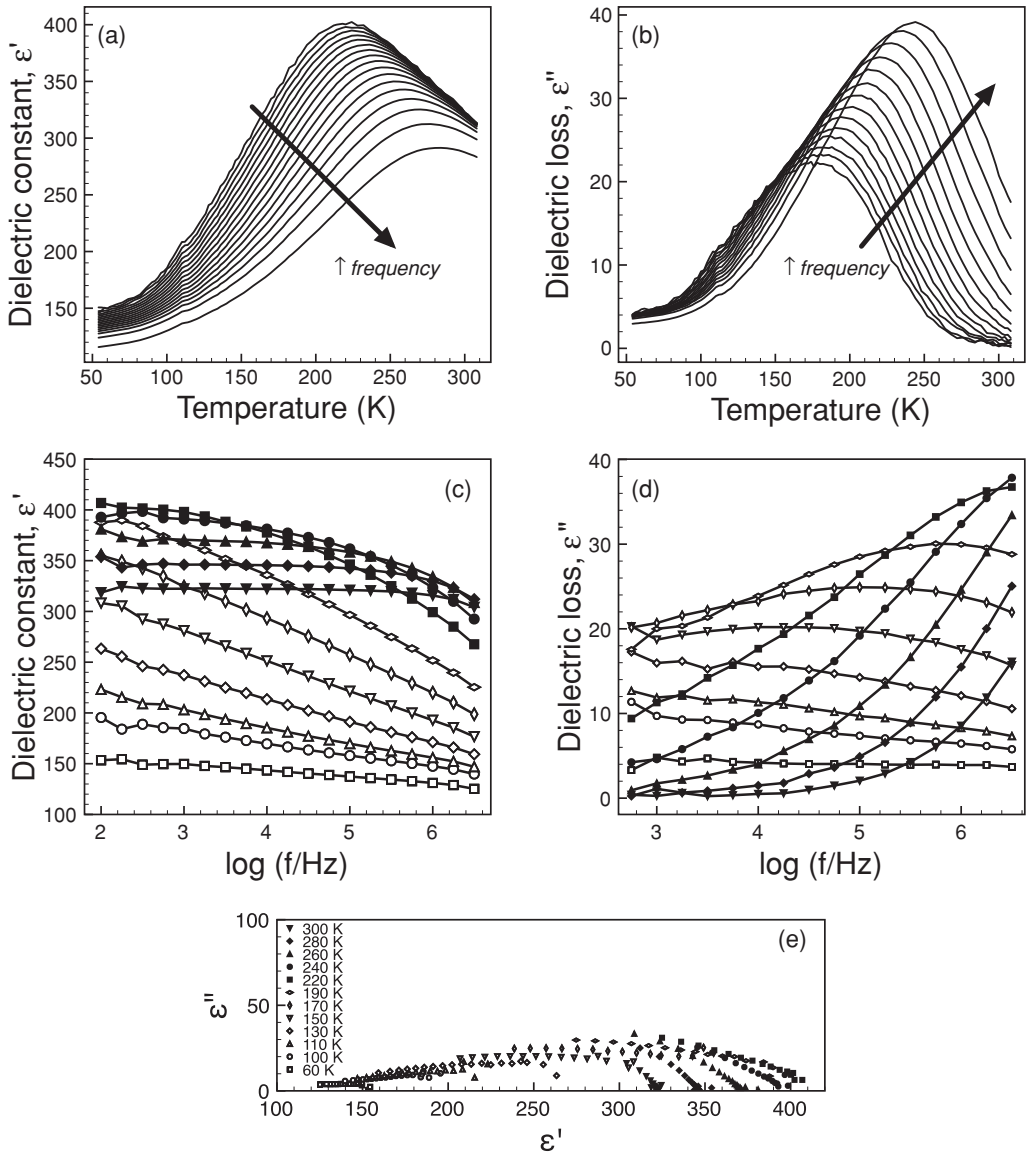

FIG. 2. Dielectric constant (a) and loss (b) as a function of frequency and temperature for $Ba_6ScNb_9O_{30}$. Real (c) and imaginary (d) components of dielectric permittivity as a function of frequency at various temperatures, and also as a Cole-Cole plot (e). The data key in part (e) also applies to parts (c) and (d).

in the neutron data collected for $Ba_6InNb_9O_{30}$. Attempts to completely remove $Ba_5Nb_4O_{15}$ secondary phase by varying synthetic conditions was unsuccessful, however, the properties of this phase are well known;[28] it is an insulator with a temperature-independent dielectric constant of ca. 40 (Refs. 28 and 29) and so has negligible contribution to the observed electrical properties of the three compositions studied.

Dielectric spectroscopy data in the range 50–400 K showed that all three compounds exhibited characteristic relaxor behavior with a strong frequency dependence of peaks in both dielectric constant and dielectric loss as a function of temperature. The dielectric curves were displaced to higher temperature with increasing average *B*-site ionic radii, as observed previously.[26] In order to further characterize this relaxor behavior data were collected with higher temperature and frequency resolution than in our previous study. Dielectric data for the Sc analog, $Ba_6ScNb_9O_{30}$, are shown in Fig. 2.

B. Analysis of dielectric data

1. Vogel-Fulcher analysis

The most commonly used method to evaluate the frequency response of the real part of dielectric permittivity in relaxors is the Vogel-Fulcher expression which was first adopted by Viehland[30] in the study of the archetypal relaxor ferroelectric, $PbMg_{1/3}Nb_{2/3}O_3$ (PMN), although there is some debate as to the validity of this approach, primarily due to problems with the goodness of fit and/or physically unreasonable fitted parameters, and this will be discussed in more detail in Sec. IV, below. The Vogel-Fulcher (VF) model essentially describes a temperature dependence of a spectrum of relaxation times and so probes the dynamics and population profile of the dipolar response(s) as a function of temperature. The VF equation (1) is simply a modified Arrhenius expression which includes

TABLE II. Vogel-Fulcher and goodness-of-fit parameters for $Ba_6M^{3+}Nb_9O_{30}$ ($M^{3+} = Ga^{3+}$, Sc^{3+}, In^{3+}) determined from data fitting in Fig. 3.

	T_{VF} (K)	f_0 (Hz)	E_a (eV)	RMSD.[a]	χ^2
$Ba_6GaNb_9O_{30}$	56.3	6.70×10^{11}	0.0768	0.0598	0.0608
$Ba_6ScNb_9O_{30}$	152.9	9.10×10^{10}	0.1052	0.1158	0.2549
$Ba_6InNb_9O_{30}$	158.3	4.05×10^{11}	0.1977	0.0532	0.0455

[a]Root mean standard deviation.

an increasing degree of interaction between random local relaxation processes, in this case of the dipolar response:

$$f = f_0 \exp\left(-\frac{E_a}{k(T_m - T_{VF})}\right), \quad (1)$$

where f is the frequency of the perturbation (applied ac field frequency, Hz); f_0 is the fundamental attempt or limiting response frequency of the dipoles (Hz); E_a is the activation energy of local polarization (J); T_m is the temperature (K) of maximum dielectric constant at frequency f; T_{VF} is the characteristic Vogel-Fulcher temperature [often described as the static freezing temperature[30] (K)]; and k is Boltzmann's constant (1.381×10^{-23} J K^{-1}).

Fits of T_m data obtained from dielectric constant curves [e.g., Fig. 2(a) to the VF expression [Eq. (1)] are shown in Fig. 3 for all three compositions. In each case the extracted parameters are all physically sensible, as shown in Table II: the fundamental attempt frequency f_0 is of the order of 10^{12} Hz (0.67, 0.09, and 0.40 THz for Ga, Sc, and In analogs, respectively); and both the activation energy E_a and Vogel-Fulcher temperature T_{VF} systematically increase with increasing B-cation size, in agreement with the less quantitative observation that the dielectric curves are displaced to higher temperature with increasing cation size.

2. *Fitting of dielectric loss*

Vogel-Fulcher analysis often results in unreliable and unphysical values for the fitting parameters[19,31,32] primarily due to the sensitivity of fitting to the curvature of $T_m(f)$ data (usually obtained over a limited frequency range, e.g., 10–10^6 Hz) and the subsequent extrapolation which is often over several orders of magnitude; our experience has also found that sample quality is also critical, particularly for polycrystalline ceramics where microstructural factors such as grain size and sample density can have a dramatic effect on the values of T_m (this will be discussed in a subsequent paper). In order to verify the parameters obtained by VF fitting of the real part of dielectric permittivity the imaginary component (dielectric loss ε'') was also analyzed. The dielectric data in Figs. 2(a) and 2(b) are plotted in the frequency domain in Figs. 2(c) and 2(d), and as a complex plane, Cole-Cole,[33] plot [Fig. 2(e)]. The data are consistent with that observed in other relaxors, including relaxor ferroelectrics.[34–37] The theory of relaxors predicts that at the static freezing temperature the dielectric loss peak associated with the dipolar response should become infinitely broad (flat) in the frequency domain. The most simple model to analyze dielectric relaxation is the simple

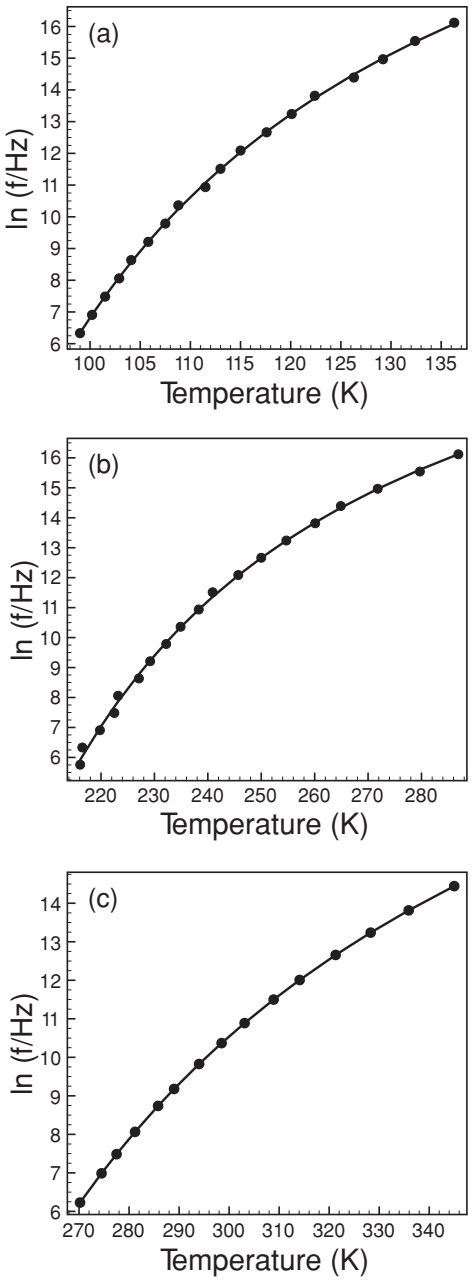

FIG. 3. Vogel-Fulcher fits of $T_m(f)$ extracted from dielectric constant data for $Ba_6GaNb_9O_{30}$ (a), $Ba_6ScNb_9O_{30}$ (b), and $Ba_6InNb_9O_{30}$ (c).

Debye response which contains a single relaxation time; this model, however, results in a symmetric loss peak with a unity relationship with frequency $\varepsilon'' \propto f^n$, where $n = -1$ and $+1$ below and above the relaxation frequency f_p, respectively. In reality, systems show more dispersive behavior and a Gaussian distribution of relaxation times (DRT) or Cole-Cole expression[33] is often introduced to fit broadened dielectric loss peaks, however, these remained symmetric about the peak relaxation frequency. The dielectric loss data as a function of frequency [Fig. 2(d)] and Cole-Cole plots [Fig. 2(e)] indicate a high degree of asymmetry, so these analytical methods are not suitable. There are a number of models to allow for asymmetric loss peaks such as the Cole-Davidson[38] or

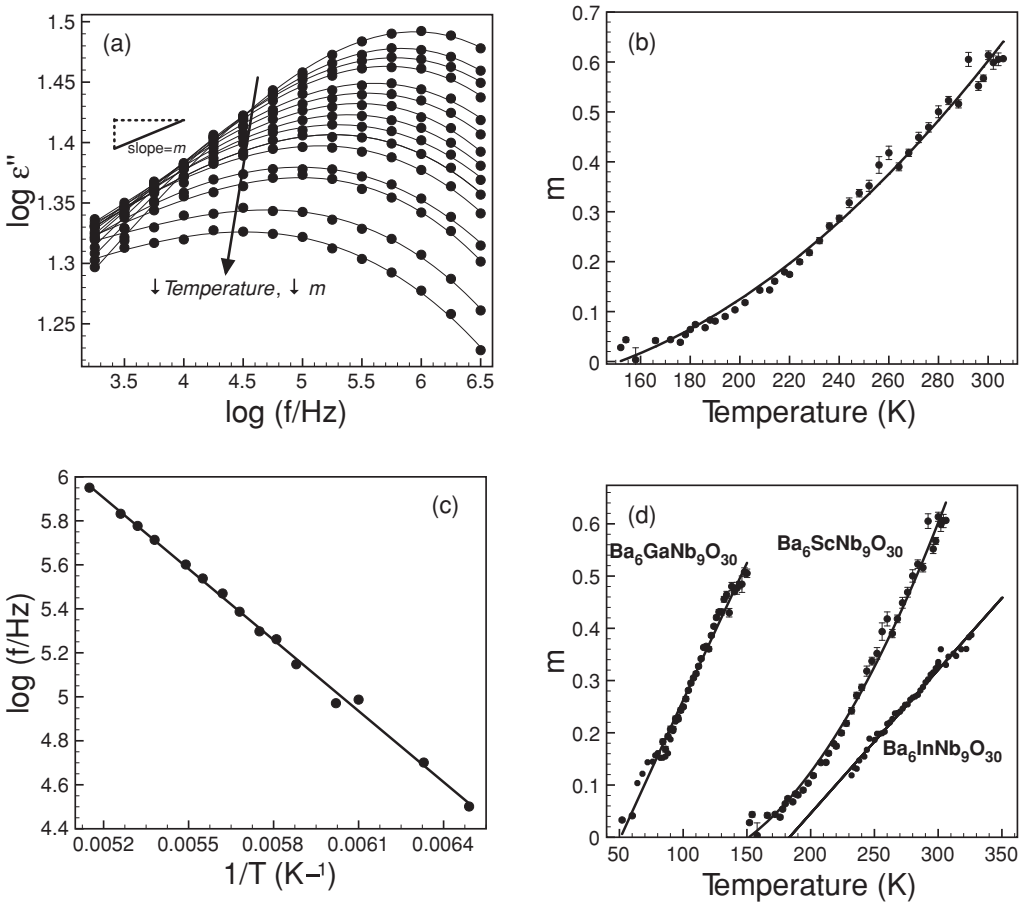

FIG. 4. Dielectric data for $Ba_6ScNb_9O_{30}$: loss peaks fitted to Jonscher's two-exponent model (a); gradient m for $\varepsilon''(f)$ at $f < f_p$ (b); and Arrhenius plot for temperature dependence of f_p (c). Comparison of m data for Ga, Sc, and In analogs (d).

Havriliak-Negami[39] expressions, however, for simplicity we have used the empirical two-exponent model of Jonscher's universal dielectric response[40] (UDR) in order to fit this $\varepsilon''(f)$ data. This approach describes the frequency dependence of dielectric loss by the expression

$$\varepsilon'' \propto \frac{1}{(f/f_p)^{-m} + (f/f_p)^{1-n}}, \tag{2}$$

where f is the ac field frequency ($=\omega/2\pi$), f_p is the relaxation (peak) frequency, and $-m$ and $(1-n)$ are the frequency exponents of $\varepsilon''(f)$ below and above f_p, respectively, with the conditions $0 \leqslant m, n \leqslant 1$. This empirical model allows a Debye response for $m = 1$, $n = 0$, and a DRT (Cole-Cole) response for $[m = (1-n)] < 1$. Furthermore, Jonscher's model also predicts that the temperature dependence of the frequency of maximum dielectric loss f_p (or dielectric relaxation frequency which is related to the relaxation time $\tau = {\omega_p}^{-1} = (2\pi f_p)^{-1}$, where ω_p is the angular frequency of the peak maxima) can be described by the Arrhenius expression

$$f_p = f_0 \exp\left(-\frac{E_a}{kT}\right), \tag{3}$$

where f_0 is the limiting dipole response frequency and E_a is the activation energy. Thus by fitting dielectric loss data to Eqs. (2) and (3), it is possible to determine some characteristic temperature, T_{UDR}, corresponding to slowing of the longest mean relaxation time by extrapolation to zero of the gradient, m ($\varepsilon'' \propto f^{-m}$ for $f < f_p$), and f_0 and E_a from the temperature dependence of f_p, respectively.

Fits to the UDR model of dielectric loss data at selected temperatures for $Ba_6ScNb_9O_{30}$ are shown in Fig. 4(a). The temperature dependence of the gradient m on the low-frequency side of the $\varepsilon''(f)$ peaks is shown in Fig. 4(b) and indicates a steady decrease in m with decreasing temperature. Absolute flattening of the loss peak (i.e., $m \to 0$) is predicted to occur at the "dipole freezing temperature";[41,42] extrapolation of the m data zero gives $T_{\mathrm{UDR}} \approx 150$ K, in comparison to T_{VF} of 153 K as determined from VF fitting of dielectric constant data. Arrhenius fitting of the temperature dependence of the peak frequency f_p is shown in Fig. 4(c), and gives values of 3.20×10^{11} Hz and 0.202 eV for f_0 and E_a, respectively. This independent treatment of both parts of the complex dielectric permittivity data gives characteristic temperature (T_{VF} or T_{UDR}), limiting frequency f_0, and activation energy E_a parameters. The rationalization of application of both Vogel-Fulcher and Arrhenius behavior is discussed in Sec. IV.

Due to the limited frequency and temperature range available and also the noise in the data, it was not possible to accurately determine $f_p(T)$ data for Ga and In analogs in order to determine f_0 and E_a using Eq. (3), however, it was possible to determine m from the gradient of the $\varepsilon''(f)$

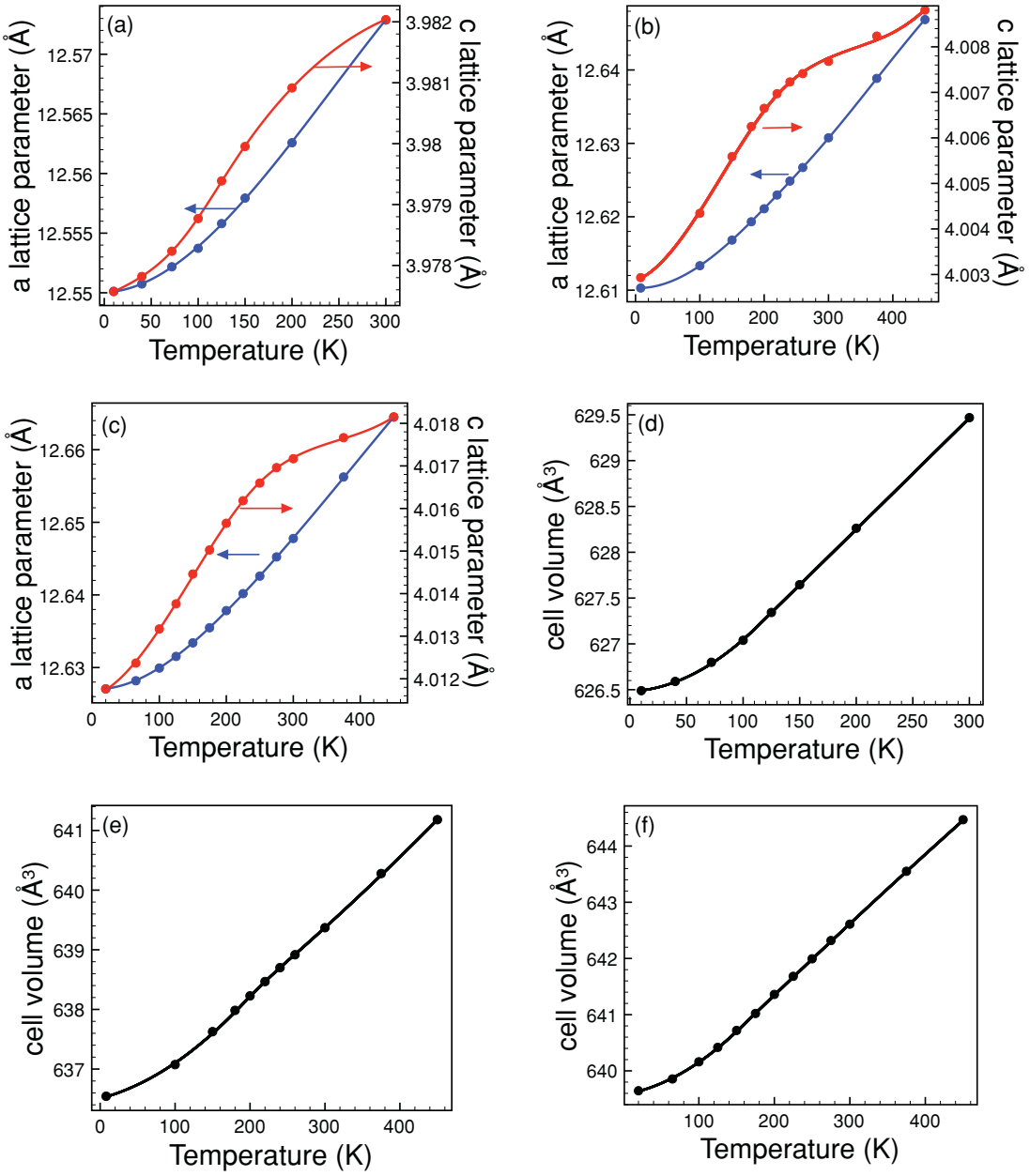

FIG. 5. (Color online) Lattice parameters and unit-cell volume as a function of temperature for $Ba_6GaNb_9O_{30}$ [(a), (d)], $Ba_6ScNb_9O_{30}$ [(b), (e)], and $Ba_6InNb_9O_{30}$ [(c), (f)] from PND data.

curves over a wide temperature range. Both samples showed similar behavior to the Sc compound with m decreasing with decreasing temperature [Fig. 4(d)]. Extrapolation of $m(T)$ curves to $m = 0$ gave $T_{UDR} = 58$ and 183 K for $Ba_6GaNb_9O_{30}$ and $Ba_6InNb_9O_{30}$, respectively, compared to T_{VF} values of 56 and 158 K from VF fitting [Fig. 3(a) and 3(c)]. It should be noted there is some uncertainty in the value of T_{UDR} for the In analog; this is discussed in Sec. IV.

C. Temperature dependence of crystal structure

Variable temperature PND in the range 450 to 8 K was used to investigate any changes in crystal structure. While some relaxor ferroelectrics such as PZN exhibit a macroscopic symmetry change,[43] others such as PMN display only local, randomly aligned (under zero-field conditions) distortions associated with local noncentrosymmetric polar nanoregions which result in diffuse scattering around the Bragg peaks.[44,45] There was no evidence of any long-range symmetry lowering at any temperature in any of the three TTB samples studied here; all data were therefore refined in the tetragonal, centrosymmetric space group $P4/mbm$. The evolution of individual lattice parameters is shown in Fig. 5. Refinement of site occupancies of M^{3+} and Nb^{5+} suggested a completely disordered system and this was supported by a significantly poorer fit to models where M^{3+} cations were constrained to either $B1$ or $B2$ sites. In all cases the materials exhibit a linear contraction in the ab plane with

TABLE III. Summary of *temperature parameters* determined from fitting of dielectric data to Vogel-Fulcher (T_{VF}) and universal dielectric response (T_{UDR}) models and from maximum tetragonality ($T_{c/a}$) determined from crystallographic data.

	$T_{c/a}$ (K)	T_{VF} (K)	T_{UDR} (K)
$Ba_6GaNb_9O_{30}$	75 ± 15	56.3	58 ± 1.5
$Ba_6ScNb_9O_{30}$	145	152.9	150 ± 2.5
$Ba_6InNb_9O_{30}$	158	158.3	183 ± 3.5

linear coefficients α, typical of oxides ($\alpha = 7.92$, 8.15, and 8.42×10^{-6} K^{-1} for Ga, Sc, and In analogs, respectively) down to ca. 100 K below which the contraction slows. As expected from the relative magnitude of the longer *a*,*b* axes compared to the *c* axis (ca. 12.6 Å vs 4 Å), this behavior dominates the volume behavior [Figs. 5(d)–5(f)]. The *c*-axis data, however, exhibit a dramatic deviation from the expected linear behavior [Figs. 5(a)–5(c)]; in each case the rate of contraction is much lower from room temperature to around 150, 200, and 250 K for Ga, Sc, and In samples, before dramatically increasing, as indicated by the strong inflexion in the data. In the approximately linear region below the inflexion $\alpha = 5.94, 5.75$, and 6.18×10^{-6} K^{-1} for Ga, Sc, and In analogs, respectively. This highly anisotropic contraction is a clear indication of some subtle structural change. It is important to note that this behavior merely reflects the average change in shape and size of the (tetragonal) unit cell and in no way reflects the local position of the atoms; this is discussed in more detail below. In our previous study we noted that the degree of anisotropy, and therefore strain (quantified by the tetragonality; i.e., ratio of c/a) showed an approximately linear relationship with T_m or T_C for *B*-site substituted relaxor or ferroelectric TTBs.[26] The crystallographic data in Figs. 5(a)–5(c) were replotted as tetragonality (c/a) (Fig. 6). All samples undergo a point of maximum tetragonality (maximum anisotropy) as a function of temperature; in each case this characteristic temperature, $T_{c/a}$, correlates with the temperatures T_{VF} and T_{UDR}, as determined from electrical analysis. A summary of the three extracted temperature parameters, T_{VF}, T_{UDR}, and $T_{c/a}$, obtained from the three methods is presented in Table III.

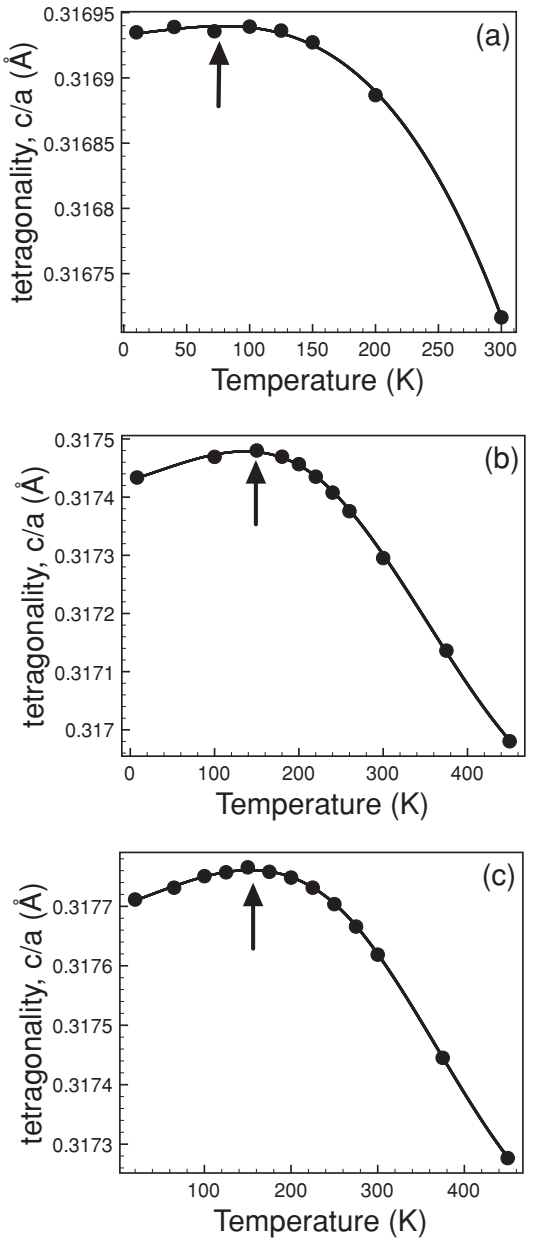

FIG. 6. Unit-cell tetragonality c/a as a function of temperature for $Ba_6GaNb_9O_{30}$ (a), $Ba_6ScNb_9O_{30}$ (b), and $Ba_6InNb_9O_{30}$ (c).

IV. DISCUSSION

A. Systematic correlation with *B*-cation size

The relaxor properties of samples were initially probed using the most common approach of fitting of the real part of dielectric permittivity to the Vogel-Fulcher model. This allowed extraction of three variables, namely, the Vogel-Fulcher temperature T_{VF}, activation energy E_a, and fundamental response frequency f_0. Where possible, E_a and f_0 parameters and characteristic temperature T_{UDR} were also determined by fitting of the dielectric loss to Jonscher's empirical two-exponent UDR model.[40] Parameters obtained from analysis of both real and imaginary parts of the complex dielectric function give good agreement Table III. The largest discrepancy is the value obtained for T_{UDR} of the In analog as determined from the extrapolation of *m* to zero [Fig. 4(d)]; this method gave a significantly higher value than the temperature extracted from the VF fitting and the crystallographic data. The extrapolation of the *m* data for this sample is from well above the expected intercept and assumes linear behavior. Similar *m* data for the Sc sample, for which it was possible to obtain *m* values over a wider temperature range, showed clear nonlinear behavior [Fig. 4(b)]; if this is also the case for the In sample, then the extrapolation used here is a significant overestimate of T_{UDR}. Unfortunately, it was not possible to obtain *m* at lower temperatures in this instance for the In analog.

Crystallographic data showed a clear structural anomaly, manifested as a maximum in anisotropy, and hence tetragonal strain at temperatures corresponding to those temperature parameters determined by two different analysis methods of dielectric data. The structural origin of this behavior is discussed

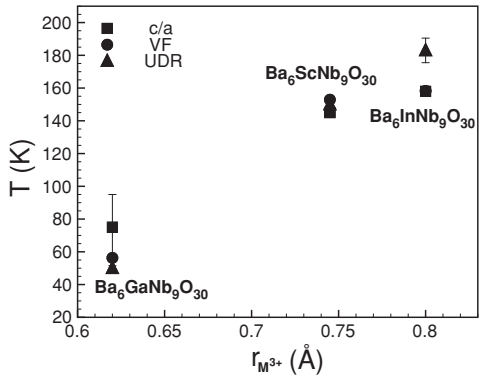

FIG. 7. Dependence of characteristic temperature parameters determined by the three different methods as a function of M^{3+} B-cation radius.

below, but what is clear is that all three samples show consistent and systematic behavior: with increasing B-cation radius the dielectric curves are displaced to higher temperatures. More in-depth analysis shows a systemic increase in the parameters E_a and, more pertinently, characteristic temperatures T_{VF}, T_{UDR}, and $T_{c/a}$ as determined from three different methods. The latter show an almost linear trend as a function of r_B (Fig. 7), as we suggested previously.[26] The overall behavior is entirely consistent with dipoles generated by an off centering of cations which decreases in magnitude with decreasing thermal energy (temperature). For the electrical response the decreasing mobility of the atomic displacements is manifested as a slowing down of the average relaxation frequency as noted in the $\varepsilon''(f,T)$ response. At $T_{c/a}$ the atoms no longer have sufficient energy to displace through the centrosymmetric position and so are locked within an energy minima in a certain crystallographic axis resulting in stiffening of the lattice and a resistance to thermal contraction. This atomistic explanation is examined in more detail in terms of the crystallographic data below. If the characteristic temperature parameters T_{VF}, T_{UDR}, and $T_{c/a}$ do indeed correspond to some dipole freezing temperature T_f, then it denotes the thermal stability of the dipoles, and is clearly related to the local crystal structure.

B. Physical manifestation of dipole freezing

There is considerable debate as to the physical meaningfulness of the parameter T_{VF} (often referred to as a dipole freezing temperature),[41,46] both because in some cases the parameters obtained for relaxor ferroelectrics and dielectrics are physically unrealistic,[31,32] and also in many polymers and glasses, for example, T_{VF} as determined from VF fitting corresponds to some seemingly arbitrary temperature below the glass transition temperature T_g, determined by thermal analysis. One would naturally assume in the latter, glassy systems that T_g and T_{VF} would coincide as the T_g describes the temperature at which "molecular" or segmental motion ceases (freezes).

It is clear in our materials, however, that T_{VF} as determined from the macroscopic, but dynamic dielectric response corresponds to a physical process which is manifested in the macroscopic, time- and spatially averaged crystal structure determined by diffraction. This indicates that T_{VF} relates to a physical process. The crystallography shows a clear and unambiguous relationship between maximal tetragonal strain and T_{VF}; this behavior is entirely consistent with the freezing of dipoles which originate from atomic displacements.

In our analysis there remains the question as to why the dielectric constant data are best described by the Vogel-Fulcher expression (a modified Arrhenius with some finite thermal activation temperature T_{VF}) while the dielectric loss displays simple thermally activated (Arrhenius) behavior (although it should be noted that it was only possible to obtain f_p values over a narrow temperature range [Fig. 4(c)]). Such behavior was previously observed in the related TTB $Sr_2LaTi_2Nb_3O_{15}$,[35] however, the authors clearly identified two contributing relaxations in the dielectric loss which they attributed to a breathing and flipping mechanism of PNRs. We do not see such a double contribution in our samples and so there are two possibilities for the observed behavior: (i) there are two separate relaxation processes: one dominates the dielectric polarizability and the other the loss, but which are not resolvable; (ii) a single mechanism gives rise to the behavior observed in both the real and imaginary parts. The first scenario may be unlikely given that the T_{VF} and T_{UDR} temperatures linked to two separate responses are coincident in each sample yet vary significantly across the compositional series. The second scenario can be rationalized based on the description of atomic displacements outlined in the previous section. The maxima in dielectric constant represent contributions of displacements through the centrosymmetric position ($z = 0.5$ in the unit cell), i.e., flipping, and T_{VF} represents the temperature at which they no longer have sufficient energy (thermal or field driven) to do so; they become locked in the c axis but are still prone to small perturbation both along the c axis (but not through the point of inversion symmetry), i.e., breathing, and in the ab plane. This behavior is akin to a flipping and breathing-type model but for non- or weakly interacting dipoles rather than collective behavior within PNRs for which we have no evidence (see discussion below). This accounts for both a freezing-type behavior for polarizability (and hence Vogel-Fulcher) behavior and finite but slowing relaxation of the dielectric loss at all temperatures.

C. Structural origin of the dipolar response

Many relaxor dielectrics differ from classical ferroelectrics in that they undergo no macroscopic change in symmetry even if there is local noncentrosymmetry as in the polar nanoregion (PNR) model, e.g., in PMN. Nevertheless, even in PMN there are some structural correlations associated with the nucleation and growth of such PNRs. For example, the local rhombohedral distortion in the PNRs with polarization developed along the ⟨111⟩ axis results in weak and diffuse Bragg scattering.[44,45] It also results in a resistance to linear thermal contraction as a result of the strain induced by the local dipoles. In zero-field-cooled (ZFC) PMN the strain induced during random nucleation of PNRs in the eightfold ⟨111⟩ directions on cooling from the high-temperature cubic polymorph spatially average resulting in an isotropic relative expansion.[44] While there is no evidence of any diffuse Bragg peaks, a similar nonlinear volume contraction at low temperature is observed. However, this only occurs below 100 K (several hundred K

TABLE IV. Goodness-of-fit parameters and U_{aniso} for the Nb1 and Nb2 sites refined in the space group $P4/mbm$ showing the large displacement in the U_{33} parameter (particularly on the $B1$ site) consistent with the anisotropy observed in the c axis.

Parameters	$Ba_6GaNb_9O_{30}$	$Ba_6ScNb_9O_{30}$	$Ba_6ScNb_9O_{30}$
χ^2	8.526	10.49	8.981
wR_p (%)	4.89	5.27	5.36
R_p (%)	4.63	4.85	4.72
a (Å)	12.55351(3)	12.61249(3)	12.62929(3)
c (Å)	3.97861(2)	4.00406(1)	4.01288(2)
Cell volume (Å^3)	626.992(3)	636.945(3)	640.051(3)
Nb1/M^{3+}1, (0,$\frac{1}{2}$, $\frac{1}{2}$)			
Nb1/ M^{3+}1 $U_{\text{aniso}} \times 100$ Å^2			
U_{11}	0.43(5)	0.40(5)	0.02(5)
U_{22}	0.43(5)	0.40(5)	0.02(5)
U_{33}	2.1(1)	3.18(9)	2.8(1)
U_{12}	−0.07(7)	−0.03(6)	0.06(7)
U_{13}	0.0	0.0	0.0
U_{23}	0.0	0.0	0.0
Nb2/ M^{3+}2 (x,y, $\frac{1}{2}$)	0.07472(7)	0.07556(6)	0.07605(7)
	0.21450(6)	0.21421(5)	0.21412(7)
Nb2/ M^{3+}2 $U_{\text{aniso}} \times 100$ Å^2			
U_{11}	0.64(4)	0.43(4)	0.56(5)
U_{22}	0.13(4)	0.08(4)	0.22(4)
U_{33}	1.00(4)	0.92(3)	1.04(4)
U_{12}	0.11(4)	0.12(3)	0.29(4)
U_{13}	0.0	0.0	0.0
U_{23}	0.0	0.0	0.0

lower than in PMN, which shows a deviation starting at the Burns temperature which is associated with PNR nucleation, and which also results in deviation from Curie-Weiss behavior and a change in refractive index)[47–50] and appears to occur at a similar temperature in all materials independent of the M^{3+} ion and therefore most likely denotes the approaching limit for bond contraction. The crystallographic data also show, however, a clear structural anisotropy at $T_{c/a}$, which is dominated by the nonlinear c-axis response. This clearly suggests that the dipoles (displacements) are (predominantly) active in the c axis. It is worthy to note that it is simply as a result of the highly anisotropic nature of the TTB structure that this distinction is clear; the majority of diffraction studies of relaxor dielectrics are perovskite based and have pseudocubic local distortions which are spatially averaged and so make identification of the displacement axis difficult using long-range, structure-averaging diffraction techniques. In order to further investigate any displacive origin of the dipoles the diffraction data were examined in more detail.

Initial refinements were carried out in the centrosymmetric, $P4/mbm$ space group with atomic displacement parameters refined isotropically (U_{iso}); these criteria confine the B cations in the c axis (to $z = 1/2$ in the unit cell) but allow displacement from their ideal positions in the ab plane (full crystallographic models may be found in the supplemental material[57]). The refinements indicate that the U_{iso} values for the $B1$ site and the oxygen ions that link the MO_6 octahedra in the c plane (O_1 and O_3) appear higher than those determined for the other ions within the unit cell. The data were refined again (in the $P4/mbm$ space group) but with anisotropic atomic displacement parameters, U_{aniso}, for the two B-site positions. All refinements showed improved goodness-of-fit factors as a result of the extra degrees of freedom associated with U_{aniso} (see supplemental material[57]). The results clearly show a large anisotropy for the $B1$ cation with much larger displacements in the c axis as indicated by U_{33}. Table IV gives the goodness-of-fit factors and U_{aniso} for the Nb_1 and Nb_2 positions for the $Ba_6GaNb_9O_{30}$, $Ba_6ScNb_9O_{30}$, and $Ba_6InNb_9O_{30}$ at 100 K (all other data is given in the supplemental material[57]). This strongly suggests that the dipoles originate from the displacement of $B1$ cations in the c axis. In an attempt to more closely estimate the magnitude of these displacements, refinements were carried out in the noncentrosymmetric space group $P4bm$; the mirror plane perpendicular to the c axis at $z = 0.5$ is removed allowing off centering of the B cations. These refinements were conducted fixing the A-site cations at the origin and in the z direction for the $A1$ and $A2$ sites, respectively, to allow the atomic displacements of the B-site cations to be quantified. There is very little movement of the Ba^{2+} ion on the $A2$ site in either the x or y directions as a result of fixing these crystallographic sites. Similarly, very little displacement is observed for the O^{2-} ions (particularly in the z direction) while there is a very clear displacement of the B-site cations.

The B-cation atomic displacements are shown visually in Fig. 8 at a temperature of 100 K. (In $P4/mbm$ symmetry the B-cations are constrained on the solid line in the center). Close inspection of the MO_6 octahedral units (Fig. 8) suggests that while the ions in the $B2$ site are displaced predominantly in the c direction, they are also (more weakly) displaced in the ab plane. This suggests that rather than being significantly linked to dipolar behavior, this displacement arises as a

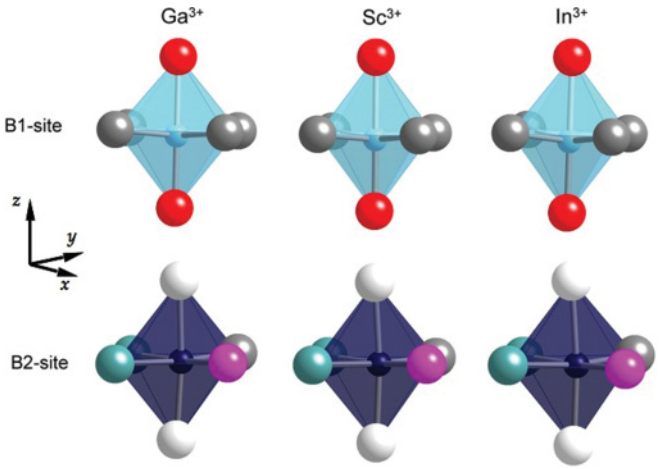

FIG. 8. (Color online) *B*-cation displacements for both *B*1 and *B*2 octahedra in Ga, Sc, and In analogs determined from refinement of data at 100 K in noncentrosymmetric space group *P*4*bm*.

result of structural distortion and a rotation of the MO_6 (*B*2) octahedra (see supplemental material[57]). On the other hand, the *B*1 octahedral site shows a clear displacement in the *c* direction consistent with a dipole moment. These results would suggest that the *B*1 site dominates the dipolar response in these materials. Unsurprisingly (as suggested by the $T_{c/a}$ values), the magnitude of displacement increases with increasing M^{3+} ionic radii, confirming the relationship between crystallographic strain and polar stability.[26]

D. Nature of the relaxor behavior

The precise nature of the relaxor behavior in these materials is not currently known. There are two broad categories of relaxor depending on the degree and length scale of correlation between the dipoles: canonical relaxor dielectrics, which are essential dipole glasses with weak dipole-dipole interactions and little or no dipole ordering, and relaxor ferroelectrics with short-range polar ordering resulting in ferroelectrically active nano-domains (commonly referred to as PNRs). The data reported here clearly indicate that these materials are essentially uniaxial relaxors with the dipolar response dominant in the short *c* axis.

Recently, the random-field Ising model (RFIM) similar to that used to explain spin-glass systems has been used to describe uniaxial relaxor character in $Sr_{0.61}Ba_{0.39}Nb_2O_6$ (SBN) tetragonal tungsten bronzes.[51] In SBN the relaxor ferroelectric character arises as a result of the formation of metastable PNRs which are separated by paraelectric interfaces. The formation of PNR occurs as a result of *A*-site disorder driven not only by the size differences between Ba^{2+} and Sr^{2+} but also by the random distribution of vacant sites.[51] The formation/random distribution of these vacancies is suggested to create random electric fields which favor the alignment of polarized clusters. Our materials incorporate neither *A*-site disorder nor vacancies. Furthermore, PND data suggests that the dipolar response in these materials is predominantly linked to the *B*1 site making these materials chemically dilute (the ratio of *B*1 to *B*2 sites is 1:4 in the TTB unit cell). This would suggest that the RFIM does not accurately describe the origin of the relaxor behavior in $Ba_6M^{3+}Nb_9O_{30}$ materials. In these TTBs it can be considered that we have a dilute dipolar system arising from "polar" chains of *B*1 ions spatially separated within an effectively nonpolar/weakly polar matrix formed by the crystallographic distribution of the *B*2 sites. While the Ising model describes uniaxial relaxor behavior, it is based on domain formation (as described above) and thus cannot describe the behavior seen here since the formation of large polar domains is restricted by the crystallography. In an attempt to investigate any relaxor ferroelectric properties in these materials, polarization-field (P-E) measurements were carried out on the $Ba_6InNb_9O_{30}$ samples at 288–298 K (i.e., well within the range of T_m values) in the frequency range 1 Hz–1 kHz and at applied fields of up to 50 kV/cm; the response was consistent with a (slightly lossy) linear dielectric. In relaxor ferroelectrics such as PMN, even at T_m and above, the residual PNRs result in either a slim loop or nonlinear behavior.[52] We observe neither, although the coercive field in these materials may be as high as 100 kV/cm (Ref. 53) which we were unable to sustain, and so these results are far from conclusive. In addition, field-cooled (1 kV/cm) followed by zero-field heating dielectric measurements in the Sc analog showed no change in the dielectric response. The absence of PNRs is also supported by the Curie-Weiss plots (see supplemental material[57]) which show no deviation associated with PNR nucleation at some Burn's temperature T_d. While certainly not conclusive, the absence of any hysteresis (P-E) loop or nonlinear behavior combined with the lack of variation of dielectric response on field cooling, and also the excellent Curie-Weiss behavior, collectively suggest an absence of PNRs, i.e., the behavior is not dominated by nucleation and growth, but more of a glassy freezing character; T_f could therefore represent the dipole freezing temperature denoting a transition from the ergodic into a nonergodic state characterized by divergence of the longest relaxation time.[54] This clearly favors a canonical relaxor dielectric (dipole glass) model for these materials, but this requires further investigation. Lastly, we have not investigated the possibility of an incommensurate crystal structure in our materials. Such periodic modulations result in a distribution of dipole environments and hence relaxor behavior.[55,56]

V. CONCLUSIONS

The relaxor properties of a previously reported[26] family of dielectrics, $Ba_6M^{3+}Nb_9O_{30}$ with $M^{3+} = Ga^{3+}$, Sc^{3+}, and In^{3+}, are presented in detail. The dielectric response was analyzed using Vogel-Fulcher fitting of the frequency dependence of the maxima in real part of the dielectric permittivity to obtain the characteristic parameters denoted fundamental dipole response frequency f_0, activation energy E_a, and Vogel-Fulcher temperature T_{VF}. Where possible, f_0, E_a, and characteristic temperature T_{UDR} parameters were also determined by independent fitting of the dielectric loss to Jonscher's empirical two-exponent model. In all cases the values obtained were in good agreement and were also physically sensible. Given the particular sensitivity of the VF methodology and its propensity to return nonphysical values, the latter method may provide a useful verification or even an alternative approach for characterization of relaxor behavior. Overall, the analysis of dielectric data

showed a systematic (almost linear) increase in the dipolar response of these materials with increasing M^{3+} cation size.

Crystallographic studies using variable temperature powder neutron diffraction were used to probe the structural response and showed that all three materials undergo nonlinear thermal contraction in the short c axis resulting in a maxima in tetragonality at a characteristic temperature $T_{c/a}$, correlating also to T_{VF} and T_{UDR} determined from dielectric data. Rietveld refinements show that the dipolar response is dominated by local, noncooperative displacement of $B1$ cations in the c axis. The magnitude of displacement increases with average B-cation size, and therefore crystal anisotropy, and is entirely consistent with the observed dielectric properties which suggest a linear increase in $T_{c/a}$, T_{VF}, and T_{UDR} with B-cation size. The collective behaviour suggests that the characteristic temperatures $T_{c/a}$, T_{VF}, and T_{UDR} determined form the various analyses are consistent with the slowing and eventual freezing of a dipolar response in these materials at a temperature T_f.

The crystallography unambiguously shows that in this family of materials T_f relates to a real physical process manifested as maximal crystallographic strain in the active dipolar axis and so is entirely consistent with dipole freezing. In these materials, therefore, T_f may be used as a direct metric of thermal stability of the dipoles.

Collectively, the data also strongly suggest that these materials are not relaxor ferroelectrics, but are better described by a "dipole glass"-type model and may therefore be better classified as relaxor dielectrics.

ACKNOWLEDGMENTS

The authors would like to thank the following funding organizations for support: the Royal Society for the provision of a research fellowship (for F.D.M.), the EPSRC (D.C.A. and A.R.), STFC for access to neutron facilities, Roberto Rocca Education Program, and INFLPR Bucharest (A.R.). We would also like to thank Professor Phil Lightfoot for discussions regarding crystallographic data.

*Corresponding author: finlay.morrison@st-andrews.ac.uk

[1] T. R. Shrout and S. J. Zhang, J. Electroceram. 111 (2007).
[2] N. A. Spaldin and M. Fiebig, Science **309**, 391 (2005).
[3] Y. Salto, H. Takao, T. Tani, T. Nonoyama, K. Takatori, T. Homma, T. Nagaya, and M. Nakamura, Nature (London) **432**, 84 (2004).
[4] G. Catalan and J. F. Scott, Adv. Mater. **21**, 2463 (2009).
[5] L. G. Van Uitert, J. J. Rubin, W. H. Grodkiewicz, and W. A. Bonner, Mater. Res. Bull. **4**, 63 (1968).
[6] L. G. Van Uitert, N. J. Levinstein, J. J. Rubin, C. D. Capio, E. F. Dearborn, and W. A. Bonner, Mater. Res. Bull. **3**, 47 (1967).
[7] S. H. Wemple, M. DiDomenico, and I. Camlibel, Appl. Phys. Lett. **12**, 209 (1968).
[8] P. B. Jamieson, S. C. Abrahams, and J. L. Bernstein, J. Chem. Phys. **48**, 5048 (1968).
[9] P. B. Jamieson, S. C. Abrahams, and J. L. Bernstein, J. Chem. Phys. **50**, 4352 (1969).
[10] T. S. Cheng, E. Amzallag, and M. Rokni, Ferroelectrics **3**, 57 (1971).
[11] A. Simon and J. Ravez, C. R. Chim. **9**, 1268 (2006).
[12] F. W. Ainger, J. A. Beswick, W. P. Bickley, R. Clarke, and G. V. Smith, Ferroelectrics **2**, 183 (1971).
[13] E. O. Chi, A. Gandini, K. M. Ok, L. Zhang, and P. S. Halasyamani, Chem. Mater. **16**, 3616 (2004).
[14] R. R. Neurgaonkar, J. G. Nelson, and J. R. Oliver, Mater. Res. Bull. **27**, 677 (1992).
[15] G. C. Miles, M. C. Stennett, I. M. Reaney, and A. R. West, J. Mater. Chem. **15**, 798 (2005).
[16] M. C. Stennett, G. C. Miles, J. Sharman, I. M. Reaney, and A. R. West, J. Eur. Ceram. Soc. **25**, 2471 (2005).
[17] M. C. Stennett, I. M. Reaney, G. C. Miles, A. R. West, C. A. Kirk, and I. Levin, J. Appl. Phys. **101**, 104114 (2007).
[18] Y. H. Sun, X. M. Chen, and X. H. Zheng, J. Appl. Phys. **96**, 7435 (2004).
[19] X. L. Zhu and X. M. Chen, Appl. Phys. Lett. **96**, 032901 (2010).
[20] H. Zhang, Z. Q. Liu, H. F. Liu, L. Fang, and H. X. Liu, J. Wuhan, University of Technology – Mater. Sci. Ed. **20**, 14 (2005).
[21] L. Fang, S. S. Meng, and C.-Z. Hu, J. Alloys Compd. **429**, 280 (2007).
[22] M. C. Foster, G. R. Brown, R. M. Nielson, and S. C. Abrahams, J. Appl. Crystallogr. **30**, 495 (1997).
[23] R. Brandt and H. Mueller-Buschbaum, Monatsch. Chem. **117**, 1239 (1986).
[24] E. Castel, M. Josse, D. Michau, and M. Maglione, J. Phys.: Condens. Matter **21**, 452201 (2009).
[25] M. Josse, O. Bidault, F. Roulland, E. Castel, A. Simon, D. Michau, R. Von der Muhll, O. Nguyen, and M. Maglione, Solid State Sci. **11**, 1118 (2009).
[26] D. C. Arnold and F. D. Morrison, J. Mater. Chem. **19**, 6485 (2009).
[27] R. D. Shannon, Acta Crystallogr. Sect. A: Cryst. Phys., Diffr., Theor. Gen. Crystallogr. **A32**, 751 (1976).
[28] T. A. Vanderah, T. R. Collins, W. Wong-Ng, R. S. Roth, and L. Farber, J. Alloys Compds. **346**, 116 (2002).
[29] C. Vineis, P. K. Davies, T. Negas, and S. Bell, Mater. Res. Bull. **31**, 431 (1996).
[30] D. Viehland, S. J. Jang, L. E. Cross, and M. Wuttig, J. Appl. Phys. **68**, 2916 (1990).
[31] H. L. Du, W. C. Zhou, F. Luo, D. M. Zhu, S. B. Qu, and Z. B. Pei, J. Appl. Phys. **105**, 124104(2009).
[32] F. Bahri, H. Khemakhem, M. Gargouri, A. Simon, R. Von der Muhll, and J. Ravez, Solid State Sci. **5**, 1445 (2003).
[33] K. S. Cole and R. H. Cole, J. Chem. Phys. **9**, 341 (1941).
[34] S. Kamba, V. Bovtun, J. Petzelt, I. Rychetsky, R. Mizaras, A. Brilingas, J. Banys, J. Grigas, and M. Kosec, J. Phys. Condens. Matter **12**, 497 (2000).
[35] V. Bovtun, S. Kamba, S. Veljko, D. Nuzhnyy, K. Knizek, M. Savinov, and J. Petzelt, J. Appl. Phys. **101**, 054115 (2007).
[36] V. Bovtun, S. Vejko, S. Kamba, J. Petzelt, S. Vakhrushev, Y. Yakymenko, K. Brinkman, and N. Setter, J. Eur. Ceram. Soc. **26**, 2867 (2006).

[37]J. Macutkevic, S. Kamba, J. Banys, A. Brilingas, A. Pashkin, J. Petzelt, K. Bormanis, and A. Sternberg, Phys. Rev. B **74**, 104106 (2006).
[38]D. W. Davidson and R. H. Cole, J. Chem. Phys. **19**, 1484 (1951).
[39]S. Havriliak and S. Negami, Polymer **8**, 161 (1967).
[40]A. K. Jonscher, *Dielectric Relaxation in Solids* (Chelsea Dielectrics Press, London, 1983).
[41]A. K. Tagantsev, Phys. Rev. Lett. **72**, 1100 (1994).
[42]N. J. Donnelly, R. M. Bowman, and J. M. Gregg, Phys. Rev. B **73**, 064110 (2006).
[43]J. S. Forrester, E. H. Kisi, K. S. Knight, and C. J. Howard, J Phys.: Condens. Matter **18**, L233 (2006).
[44]J. Zhao, A. E. Glazounov, Q. M. Zhang, and B. Toby, Appl. Phys. Lett. **72**, 1048 (1998).
[45]P. Bonneau, P. Garnier, G. Calvarin, E. Husson, J. R. Gavarri, A. W. Hewat, and A. Morrell, J. Solid State Chem. **91**, 350 (1991).
[46]W. M. Saslow, Phys. Rev. B **37**, 676 (1988).
[47]G. Burns and F. H. Dacol, Phys. Rev. B **30**, 4012 (1984).
[48]G. Burns and F. H. Dacol, Phys. Rev. B **28**, 2527 (1983).
[49]G. Burns and F. H. Dacol, Solid State Commun. **48**, 853 (1983).
[50]G. Burns and F. H. Dacol, Ferroelectrics **52**, 103 (1983).
[51]W. Kleemann, J. Dec, V. V. Shvartsman, Z. Kutnjak, and T. Braun, Phys. Rev. Lett. **97**, 065702 (2006).
[52]D. Fu, H. Taniguchi, M. Itoh, S. Y. Koshihara, N. Yamamoto, and S. Mori, Phys. Rev. Lett. **103**, 207601 (2009).
[53]W. Sakamoto, T. Yogo, A. Kawase, and S. Hirano, J. Am. Ceram. Soc. **81**, 2692 (1998).
[54]A. Levstik, Z. Kutnjak, C. Filipic, and R. Pirc, Phys. Rev. B **57**, 11204 (1998).
[55]M. Venet, J. C. M'Peko, F. L. Zabotto, F. Guerrero, D. Garcia, and J. A. Eiras, Appl. Phys. Lett. **94**, 172901 (2009).
[56]I. Levin, M. C. Stennett, G. C. Miles, D. I. Woodward, A. R. West, and I. M. Reaney, Appl. Phys. Lett. **89**, 122908 (2006).
[57]See supplemental material at [http://link.aps.org/supplemental/10.1103/PhysRevB.83.184302] for full crystallographic material.